Coupled-channels analysis of silicon-nickel fusion reactions

S. Landowne, Steven C. Pieper, and F. Videbaek
Physics Division, Argonne National Laboratory, Argonne, Illinois 60439
(Received 31 July 1986)

Coupled-channels calculations are carried out for the series of $^{28,30}Si+^{58,62,64}Ni$ fusion reactions. The low-lying excitations of the projectile and target nuclei are taken into account within the rotational and vibrational models, respectively. The effects of one- and two-nucleon transfer reactions are included in the calculations using approximate methods. A good overall agreement with the data is obtained. The fusion cross sections apparently reflect changes in the radii of the nickel isotopes suggested by Hartree-Fock calculations.

I. INTRODUCTION

The series of $^{28,30}Si + ^{58,62,64}Ni$ fusion reactions measured by the Legnaro group poses an interesting problem.[1] Differences are found in the subbarrier cross sections as the number of valence neutrons change which point to the need for an analysis which accounts for the structure of the colliding nuclei. Since the low-lying collective states of the nickel isotopes have similar properties, one might expect that the variations observed as the target changes are due to different probabilities for transfer reactions to occur. It was suggested in Ref. 1 that the availability of two-nucleon transfer reaction channels with positive effective Q values might account for the behavior of the subbarrier cross sections. It would also be interesting to know if the one-nucleon transfer reactions or the different deformed natures of the projectiles (oblate for ^{28}Si and prolate for ^{30}Si) play special roles in the fusion process.

In the present work we make an assessment of these various effects by carrying out a detailed coupled-channels analysis. The calculations are similar to those of Ref. 2 in that fusion is defined by imposing an ingoing-wave boundary condition on the coupled wave equations. In other words, fusion is considered to be controlled by a barrier penetration process which can be significantly modified by allowing couplings to additional degrees of freedom.[3] Within this framework it is straightforward to include the effects of low-lying surface excitation modes. The role of the transfer reactions, however, is studied in a more approximate way.[4] Since transfer reaction data are not available for these systems, we have relied on estimates of their effects, which are discussed in detail below.

In the next section we explain how the various parameters for the calculations are determined. The results are presented and commented on in Sec. III. Finally, Sec. IV gives the conclusions of this work.

II. PARAMETERS OF THE CALCULATIONS

A. The potential and the inelastic excitation couplings

The potential for the present case is complicated by the deformed nature of the silicon projectiles. We have used the macroscopic rotational model in which the nuclear ion-ion interaction is assumed to have the form

$$U_N(r) = -V_0/[1+\exp(x)] ,$$

$$x = [r - R_p'(\theta) - R_t]/a_0 ,$$

$$R_p'(\theta) = R_p[1+\beta_p Y_{20}(\theta)] ,$$

where $R_p = r_0 A_p^{1/3}$ and $R_t = r_0 A_t^{1/3}$. The central, monopole potential is obtained by averaging U_N over the intrinsic orientation θ. The higher multipoles give the coupling and reorientation interactions for the projectile excitation (see, e.g., Ref. 5). In the calculations we include the first 2^+ and 4^+ projectile states and allow for quadrupole reorientation, as indicated in Fig. 1.

The coupling scheme for the nickel excitations is also indicated in Fig. 1. The "vibrational" model in which the nuclear coupling interactions are proportional to the

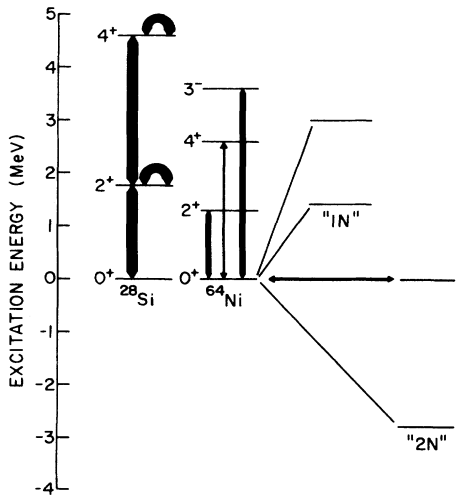

FIG. 1. Level scheme indicating the channels included in the $^{28}Si + ^{64}Ni$ calculation. The width of the lines suggest the relative strengths of the couplings in the barrier region. Similar schemes have been used for all of the Si-Ni combinations. For details, see Tables I and II.

derivative of the nuclear potential is used to describe the target excitations. For simplicity, and because the deformation parameters required to fit the inelastic scattering data were determined for a spherical potential,[6] the derivative of the undeformed Woods-Saxon potential was taken.

The parameters which specify the inelastic transitions are collected in Table I. It should be noted that they are quite similar for the three nickel isotopes. The main differences between ^{28}Si and ^{30}Si are the sign change in the deformation and a reduction in the coupling strength.

The basic potential parameters V_0, r_0 and a_0 were chosen as follows. First, we used the empirical ion-ion potential of Ref. 7, which has $a_0=0.63$ fm and yields values of $V_0\simeq 40$ MeV and $r_0\simeq 1.2$ fm for Si + Ni. This potential was satisfactory in the sense that the higher energy fusion cross sections for ^{28}Si + ^{58}Ni were well reproduced and adding the inelastic coupling brought a good agreement with the lower energy points for this system. Furthermore, this potential was similar to the one used in Ref. 6 to analyze Si + Ni elastic and inelastic scattering. However, we found that the low-energy fusion cross sections in the ^{28}Si + ^{64}Ni calculation showed unacceptable variations with respect to changes in the ingoing-wave boundary condition radius R_b. This case is distinguished by having the strongest coupling effects in the Si + Ni series. The instability was attributed to the combination of a strong coupling interaction with a relatively shallow potential. Keeping the diffusivity fixed at $a_0=0.63$ fm, we increased V_0 and decreased r_0 so as to keep the same tail as the potential of Ref. 7, and therefore nearly the same Coulomb barrier, but produce a deeper interior well. With $V_0=-100$ MeV and $r_0=1.114$ fm we obtained stable results in the presence of strong couplings. Accordingly, these were used as the reference parameters for the calculations. The ingoing boundary condition was applied at $R_b=7$ fm in all of the calculations.

TABLE I. Inelastic excitation coupling parameters. The nuclear (β_N) and Coulomb (β_C) deformations are taken to be equal.

Nucleus (model)	Transition (i-f)	ΔE (MeV)	$\beta_N=\beta_C$
^{28}Si	0^+-2^+	1.78	−0.42
(rotational)	2^+-2^+	0.0	−0.42
	2^+-4^+	2.84	−0.42
	4^+-4^+	0.0	−0.42
^{30}Si	0^+-2^+	2.24	0.30
(rotational)	2^+-2^+	0.0	0.30
	2^+-4^+	3.04	0.30
	4^+-4^+	0.0	0.30
^{58}Ni	0^+-2^+	1.45	0.20
(vibrational)	0^+-3^-	4.47	0.20
	0^+-4^+	2.46	0.12
^{62}Ni	0^+-2^+	1.17	0.20
(vibrational)	0^+-3^-	3.70	0.15
	0^+-4^+	2.33	0.10
^{64}Ni	0^+-2^+	1.34	0.19
(vibrational)	0^+-3^-	3.60	0.15
	0^+-4^+	2.62	0.05

The radius parameter $r_0=1.114$ fm was used for both ^{28,30}Si + ^{58}Ni reactions. During the course of our work it became clear that improved agreement could be obtained for the Si + ^{62,64}Ni reactions by allowing r_0 to increase. It was interesting to discover that this effect could be correlated with the neutron radii of the nickel isotopes predicted by Hartree-Fock calculations. Recent Hartree-Fock results give root-mean-square neutron radii of 3.67, 3.75, 3.82, and 3.87 fm for the ^{58,60,62,64}Ni series.[8] A similar change between ^{58}Ni and ^{64}Ni was reported earlier in Ref. 9. These radii, divided by $A^{1/3}$, are in the ratio 1/1.010/1.017/1.019. In the fusion calculations we therefore increased the ^{62}Ni and ^{64}Ni radii in the nuclear potential by 1.7% and 2% with respect to the $A^{1/3}$ scaling, respectively. The effect of such changes will be illustrated in Sec. III.

B. The transfer couplings

In addition to the inelastic excitations, we have included channels to simulate the effects of one- and two-nucleon transfer reactions. Technically, these extra channels are specified as 0^+ target states with excitation energies given by the negative of the effective Q values for the reaction.[4] Since there are many possible transfer reactions with coupling interactions which are not well known, and measurements are not available, we have relied on approximations in order to estimate their effects.

For the case of two-nucleon transfer reactions we have allowed for two channels. One of them corresponds to the ground state two-neutron transfer reaction. It is singled out because of the suggestion that the positive Q value for this reaction in some of the cases, particularly ^{28}Si + ^{64}Ni, might be responsible for the variations observed in the subbarrier fusion cross sections.[1] To estimate its strength we have used the macroscopic prescription of Ref. 10. Here the form factor is proportional to the derivative of the nuclear potential, just like an inelastic vibrational excitation. The corresponding "deformation" parameter $\beta_{\rm tr}$ is then obtained by fitting a measured transfer cross section.

Specifically, we took the value $\beta_{\rm tr}=0.05$ from the analysis of the ^{64}Ni(^{18}O,^{16}O) ground state reaction in Ref. 10 and applied it to the ^{64}Ni(^{28}Si,^{30}Si) case. It may be noted that this procedure gave consistent results for the ^{64}Ni(^{58}Ni,^{60}Ni) ground state reaction, as reported in Ref. 11. We also checked this prescription against a more microscopic ^{64}Ni(^{28}Si,^{30}Si) calculation. In this case the two-nucleon form factors were calculated using the code TWOFF.[12] A $(d_{5/2})^2$ wave function was used to describe the ^{28}Si-^{30}Si overlap and a configuration of $0.71(2p_{3/2})^2+0.89(1f_{5/2})^2+0.48(1p_{1/2})^2-1.05(1g_{9/2})^2$ was used for the ^{62}Ni-^{64}Ni overlap.[13] The resulting distorted-wave Born-approximation (DWBA) cross sections were then multiplied by an empirical factor of 8, which was the enhancement of measured cross sections over calculated ones in a similar analysis of (^{14}C,^{12}C) reactions.[14] The resulting cross sections agreed with those obtained with the simple macroscopic prescription to within a factor of 2.

We kept the strength β_{tr} fixed for all of the silicon-nickel combinations to test the effects of the varying ground state Q values. As expected, the cases with more positive Q values had the largest effects on the low-energy fusion rates.[3] However, on an absolute scale these effects are small for the present series of reactions, and confined to the very low energy region, so that the large variations observed cannot be ascribed to the presence of this one particular transfer channel.

We then noted from data systematics that the total two-neutron transfer cross section should be much larger than the ground state transfer.[15] Consequently, we included an additional channel at an excitation energy of about 3 MeV with respect to the ground state Q value for ^{64}Ni(^{28}Si,^{30}Si) and adjusted the strength parameter up to $\beta_{tr}=0.15$, so as to have an order of magnitude compatible with the bulk of other known two-neutron transfer reactions. The choice of 3 MeV for the excitation energy was made from considering an unpublished spectrum for the ^{48}Ca(^{28}Si,^{30}Si) reaction. It should be emphasized that this prescription is a rough attempt to account for the low-lying two-nucleon transfer strength. It would be interesting to have measurements of these transfer reaction cross sections.

The above procedure was followed for each of the six cases. The various parameters for the couplings are summarized in Table II. Notice that describing the bulk of the two-neutron transfer in this way corresponds to adding a channel with a strength as large as the 3^- coupling in the nickel isotopes, but the excitation energy varies as the ground state Q value changes. This leads to significant effects on the fusion cross sections for the cases with the most positive ground state Q values.

TABLE II. Transfer reaction coupling parameters.

System	Type	Q (MeV)	β (F)[a]
^{28}Si + ^{58}Ni	1N	−4.0	(1.1)
	2N	−3.2	0.05
	2N	−6.0	0.15
^{28}Si + ^{62}Ni	1N	−3.0	(3.0)
	2N	+0.8	0.05
	2N	−2.0	0.15
^{28}Si + ^{64}Ni	1N	−1.4	(1.4)
	1N	−3.0	(2.7)
	2N	+2.8	0.05
	2N	0.0	0.15
^{30}Si + ^{58}Ni	1N	−2.8	(3.0)
	2N	+1.2	0.05
	2N	−1.6	0.15
^{30}Si + ^{62}Ni	1N	−4.8	(3.0)
	2N	−2.5	0.05
	2N	−5.3	0.15
^{30}Si + ^{64}Ni	1N	−4.0	(3.0)
	2N	−0.5	0.05
	2N	−3.3	0.15

[a]One-nucleon (1N) couplings are computed as $V=F/\{1+\exp[(r-R)/a]\}$ MeV, where $R=1.2(A_p^{1/3}+A_t^{1/3})$ fm and $a=1.4$ fm. Two-nucleon (2N) couplings are computed as $V=(\beta R/\sqrt{4\pi})dU/dr$, where U is the spherical nuclear potential (see text) and $R=1.114A_t^{1/3}$ fm. The last column gives either β or, in parentheses, F.

The plots of the effective Q values for the various transfer reactions shown in Fig. 2 help one to appreciate where the transfer strength lies. Here the effective Q value is defined as the ground state Q value plus the difference between the Coulomb barriers in the entrance and exit channels, computed as in Ref. 16. For the ^{28}Si series, the Q values become more positive as the target mass increases. The trend follows a different pattern for the ^{30}Si reactions. The ^{30}Si + ^{62}Ni Q values are the most negative ones of this series. It is shown in the next section how the enhancement of the subbarrier fusion due to transfer reflects these variations.

We have also investigated the effects of one-nucleon transfer reactions. First of all, we carried out detailed finite-range DWBA calculations, using known spectroscopic factors, for the most important single-nucleon transfer reactions in the ^{28}Si + ^{58}Ni and ^{28}Si + ^{64}Ni systems. The results of the calculations at $E_{c.m.}=55$ MeV are summarized in Table III. It may be noted that the total strength for ^{28}Si + ^{64}Ni is over an order of magnitude larger than for ^{28}Si + ^{58}Ni. The DWBA calculations account for about 60% of the single-nucleon transfer strength expected from systematics at an energy 1.25 times the Coulomb barrier.[15]

To incorporate this information into the coupled-channels fusion calculations, we added an additional state at an average Q value with a coupling interaction designed to account for the strength of the DWBA calculations. For the ^{28}Si + ^{58}Ni case, a channel with a Q

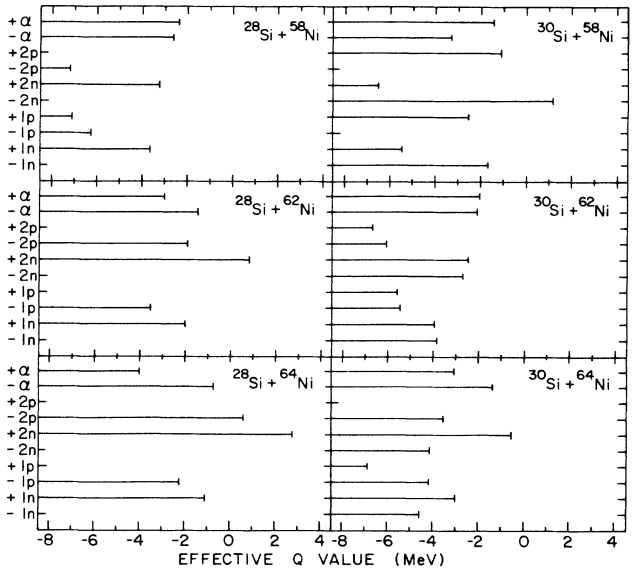

FIG. 2. Range of Q values for one- and two-nucleon and alpha-particle transfer reactions induced by ^{28}Si + ^{58,62,64}Ni and ^{30}Si + ^{58,62,64}Ni. The reaction type is indicated on the vertical axis (−1 for one neutron stripping, +2p for two proton pick-up, etc.). The corresponding horizontal bars end at the value of the effective ground state Q values for the reaction (see text).

value of -4 MeV was included. For the $^{28}Si + {}^{64}Ni$ calculations we used two channels with Q values of -1.4 and -3.8 MeV to account for the fractionated transfer strength in this case (see Table III).

The corresponding coupling interactions were parametrized with the form

$$V_{tr} = F_{tr}/[1+\exp(x_{tr})] ,$$

$$x_{tr} = [r - r_{tr}(A_p^{1/3} + A_t^{1/3})]/a_{tr} .$$

Keeping $r_{tr} = 1.2$ fm, the strength and diffusivity parameters were adjusted in the coupled-channels calculations to agree with the total magnitude and angular distribution of the DWBA "data." We found $a_{tr} = 1.4$ fm, which is a typical decay length corresponding to one-nucleon separation energies. The strength parameters are $F_{tr} = 1.1$ MeV for the ^{58}Ni case and $F_{tr} = 1.4$ and 2.8 MeV for the two ^{64}Ni cases, respectively. The curves in Fig. 3 show a comparison between DWBA and coupled-channels calcula-

TABLE III. Total cross sections from DWBA calculations for $^{28}Si + {}^{58,64}Ni$ single-nucleon transfer reactions at $E_{c.m.} = 55$ MeV. The optical parameters are $V = 37.5$ MeV, $W = 24.1$ MeV, $r_0 = r_i = 1.2$ fm, and $a_0 = a_i = 0.695$ fm, from Ref. 6. The spectroscopic factors for the residual and ejectile states are S_T and S_P, respectively. The bound-state wave functions were generated in a Woods-Saxon well with a radius parameter of $r_0 = 1.25$ fm for Ni and Cu states and $r_0 = 1.20$ fm for Si and Al states. The diffusivity was 0.65 fm and the strength of the spin-orbit interaction was 7 MeV.

Residual	Ejectile	S_T	S_P	E_x (MeV)	σ (mb)
^{63}Ni[a]	^{29}Si[b]		($Q_{gg} = -1.18$ MeV)		
$2p_{1/2}$ g.s.	$1s_{1/2}$ g.s.	0.47	0.55	0.0	2.93
$1f_{5/2}$ 0.087	$1s_{1/2}$ g.s.	3.43	0.55	0.087	3.17
$2p_{3/2}$ 0.156	$1s_{1.2}$ g.s.	2.42	0.55	0.156	15.21
$2p_{3/2}$ 0.518	$1s_{1/2}$ g.s.	0.82	0.55	0.520	4.55
$2p_{1/2}$ 1.001	$1s_{1/2}$ g.s.	0.52	0.55	1.00	0.89
$2p_{1/2}$ g.s.	$1d_{3/2}$ 1.27	0.47	1.00	1.27	0.74
$1g_{9/2}$ 1.292	$1s_{1/2}$ g.s.	0.80	0.55	1.29	0.22
$1f_{5/2}$ 0.087	$1d_{3/2}$ 1.27	3.43	1.00	1.36	0.30
$2p_{3.2}$ 0.756	$1d_{3/2}$ 1.27	2.42	1.00	1.43	11.40
$2p_{3/2}$ 0.518	$1d_{3/2}$ 1.27	0.82	1.00	1.79	2.61
$1f_{5/2}$ 1.790	$1s_{1/2}$ g.s.	0.20	0.55	1.79	0.05
$1f_{7/2,5/2}$ 1.900	$1s_{1/2}$ g.s.	0.45	0.55	1.90	≈ 0.2
$2p_{1/2}$ g.s.	$1d_{5/2}$ 2.03	0.47	0.19	2.08	0.47
$1f_{5/2}$ 0.087	$1d_{5/2}$ 2.03	3.43	0.19	2.12	1.02
$1p_{3/2}$ 2.14	$1s_{1/2}$ g.s.	0.36	0.55	2.14	0.39
$2p_{3/2}$ 0.156	$1d_{5/2}$ 2.03	2.42	0.19	2.19	1.27
$1g_{9/2}$ 2.52	$1s_{1/2}$ g.s.	0.20	0.55	2.51	0.04
$2p_{1/2}$ 1.001	$1d_{3/2}$ 1.27	0.52	1.00	2.27	1.23
$1g_{9/2}$ 1.292	$1d_{3/2}$ 1.27	0.80	1.00	2.56	0.49
$1f_{7/2,5/2}$ 1.90	$1d_{3/2}$ 1.27	0.45	1.00	3.17	0.18
					$\Sigma = 47.01$
^{65}Cu[c]	^{27}Al[b]		($Q_{gg} = -4.13$ MeV)		
$2p_{3/2}$ g.s.	$1d_{5/2}$ g.s.	0.72	3.05	0.0	3.48
$2p_{1/2}$ 0.77	$1d_{5/2}$ g.s.	0.65	3.05	0.77	0.65
$2p_{3/2}$ g.s.	$2s_{1/2}$ 0.84	0.77	0.60	0.84	1.52
$1f_{5/2}$ 1.11	$1d_{5/2}$ g.s.	0.19	3.05	1.11	0.43
					$\Sigma = 6.08$
^{57}Ni[d]	^{29}Si[b]		($Q_{gg} = -3.72$ MeV)		
$2p_{3/2}$ g.s.	$2s_{1/2}$ g.s.	1.04	0.55	0.0	0.90
$1f_{5/2}$ 0.768	$2s_{1/2}$ g.s.	1.05	0.55	0.768	0.062
$2p_{1/2}$ 1.112	$2s_{1/2}$ g.s.	0.21	0.55	1.112	0.05
$2p_{3/2}$ g.s.	$1d_{3/2}$ 1.27	1.04	1.00	1.27	0.35
$1f_{5/2}$ 0.768	$1d_{3/2}$ 1.27	1.05	1.00	2.04	0.002
$2p_{3/2}$ g.s.	$1d_{5/2}$ 2.03	1.04	0.19	2.03	0.002
					$\Sigma = 1.37$

[a]Reference 17.
[b]Reference 18.
[c]Reference 19.
[d]Reference 20.

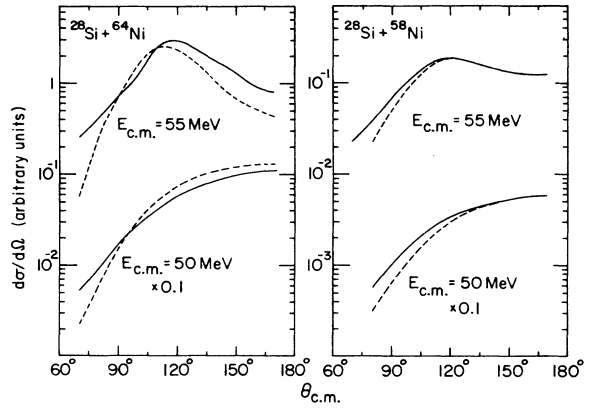

FIG. 3. Comparison of finite-range DWBA one-nucleon transfer calculations (solid curves) with parametrized coupled-channel results (dashed curves) for $^{28}Si + ^{64}Ni$ and $^{28}Si + ^{58}Ni$ induced reactions at two bombarding energies.

tions for one-nucleon transfer reactions. Considering the simplicity of the parametrizations, the overall agreement is quite good.

It turns out that in spite of the fact that the calculated single-nucleon transfers have relatively large cross sections, their effect on the fusion results are rather small. Accordingly, we took an expediant approach for the other silicon-nickel systems. In each of these cases we allowed one channel at 1 MeV excitation energy with respect to the ground state Q value and with a strength of $F_{tr}=3$ MeV. The various parameters for the transfer couplings are summarized in Table II.

III. RESULTS OF THE FUSION CALCULATIONS

The results of the fusion calculations for the complete series of $^{28,30}Si + ^{58,62,64}Ni$ reactions are presented in Figs. 4–6. In each figure we also show the predicted cross sections for one- and two-nucleon transfer reactions. The one-nucleon transfer cross sections for $^{28}Si + ^{58}Ni$ and $^{28}Si + ^{64}Ni$ should be more reliable since they reproduce detailed microscopic calculations. In any case the transfer predictions should be considered as order of magnitude estimates for the strengths at excitation energies less than about 5 MeV. This is the region which is expected to be most important when analyzing the effects of transfer reactions on the subbarrier fusion rates.

The overall agreement with the fusion data is good, including the higher energy regions which depend sensitively on the nuclear potential and the lower energies which reflect the coupling interactions. This can be appreciated in each figure by considering the dashed curves which show the no-coupling limits. The dotted curves show the results when only the inelastic excitation channels are included. The differences between these and the solid curves are due to the transfer reaction couplings.

It is seen that the inelastic excitation couplings enhance the subbarrier fusion cross sections significantly and approximately by the same amount in each case. This reflects the similarity of the low-lying spectra of the dif-

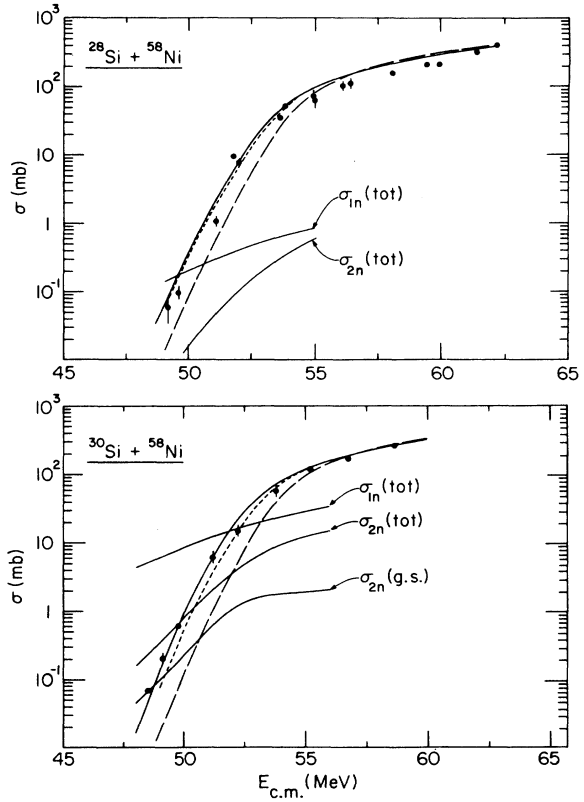

FIG. 4. Calculated fusion and transfer reaction cross sections for the $^{28,30}Si + ^{58}Ni$ systems. The fusion data are from Ref. 1. The dashed curves show the no-coupling limit. Including inelastic excitation channels gives the dotted curves and further adding the transfer channels gives the solid curves.

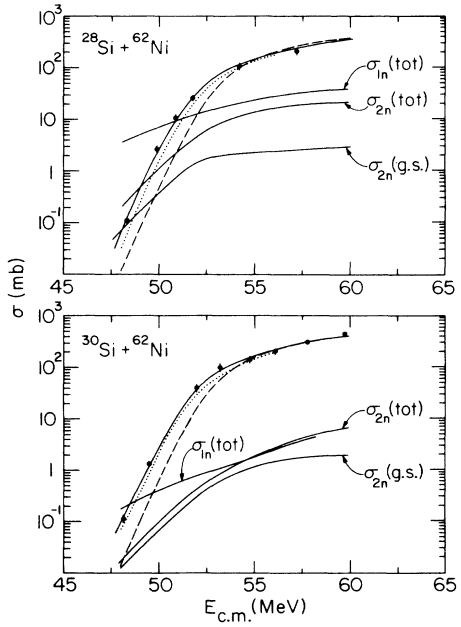

FIG. 5. Calculated fusion and transfer reaction cross sections for the $^{28,30}Si + ^{62}Ni$ systems. The fusion data are from Ref. 1. The curves are explained in the caption of Fig. 4.

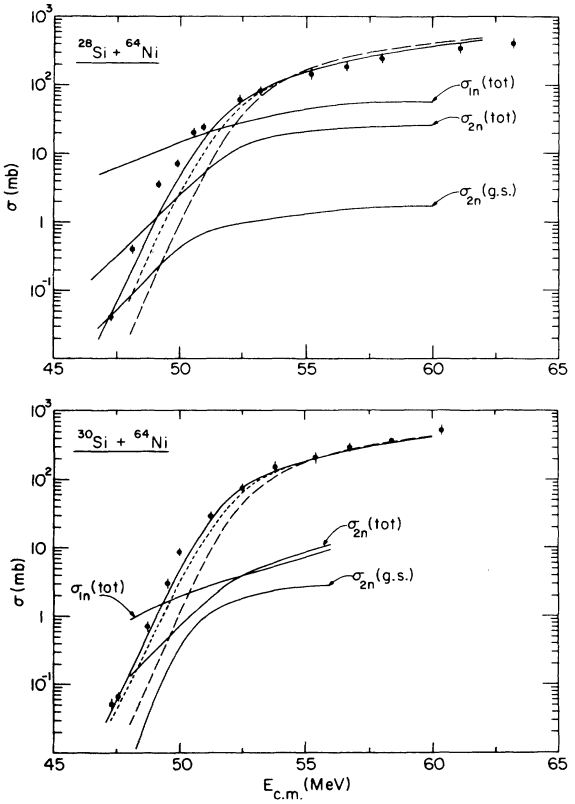

FIG. 6. Calculated fusion and transfer reaction cross sections for the ^{28,30}Si + ^{64}Ni systems. The fusion data are from Ref. 1. The curves are explained in the caption of Fig. 4.

ferent isotopes. The largest single effect comes from the strong projectile excitation.

The enhancement due to inelastic excitations is sufficient to explain the low-energy fusion data for ^{28}Si + ^{58}Ni, as shown in Fig. 4. It is consistent that the transfer reactions are predicted to have low cross sections in this case and that their influence on the subbarrier fusion is negligible. On the other hand, the inelastic couplings are clearly insufficient to explain the low-energy fusion cross sections for ^{28}Si + ^{64}Ni in Fig. 6. Here the largest transfer reaction cross sections are expected and their effects are necessary to obtain the agreement shown. Indeed, it appears that additional transfer strength may be required in this case. The intermediate case of the ^{28}Si + ^{62}Ni reaction in Fig. 5 is well reproduced by the combined effects of inelastic and transfer reaction couplings.

Some interesting details can be seen by comparing the series of ^{30}Si induced reactions to those initiated by ^{28}Si. The agreement with the higher energy ^{30}Si fusion data indicates that the deformed potential with the usual radial scaling, and no additional free parameters, is able to account for the difference between ^{30}Si and ^{28}Si. We have checked that the oblate ^{28}Si deformation reduces the subbarrier fusion, while the prolate deformation of ^{30}Si increases it. The systematic agreement with the low-energy data would be disturbed if the wrong signs of deformation parameters were used. However, the absolute effects due to these projectile shape changes are small for the reactions studied here. For example, switching the sign of projectile deformation parameter in the ^{28}Si + ^{64}Ni calculation at $E_{c.m.} = 50$ MeV causes the fusion cross section to increase from 4.6 to 6.6 mb. Part of this effect is due to the change in the central potential since the cross section in the no-coupling limit also increases, from 0.92 to 1.1 mb.

It is interesting to note in Fig. 4 that while the inelastic couplings alone bring agreement with the low-energy ^{28}Si + ^{58}Ni data, the corresponding ^{30}Si + ^{58}Ni calculations underpredict the low-energy cross sections. This discrepancy is removed by including the transfer reactions, which are predicted to be larger than for ^{28}Si + ^{58}Ni. The opposite effect is seen when comparing the ^{28,30}Si + ^{62}Ni systems. The transfer Q values are not favorable for the ^{30}Si + ^{62}Ni case (see Fig. 2). One sees that the effect of the transfer channels on the subbarrier fusion is more pronounced for ^{28}Si + ^{62}Ni.

It should be pointed out that even though the one-nucleon transfer cross sections are predicted to be larger than those for two-nucleon transfer, the latter produce a greater enhancement effect on the subbarrier fusion in all of the cases studied here. In addition, the bulk of the two-nucleon transfer is more effective in enhancing the fusion than the ground state transition in our calculations. The variations in the fusion calculations due to the transfer couplings mainly reflect the different Q values assigned to the bulk of the two-nucleon transfer strength.

For example, consider the case of ^{28}Si + ^{64}Ni, which has the largest one- and two-nucleon transfer cross sections. When the one-nucleon transfer couplings are switched off, the calculated fusion cross section at $E_{c.m.} = 50$ MeV decreases from 4.6 to 3.9 mb. Further removing the two-nucleon transfer channels causes a larger reduction, from 3.9 to 2.7 mb. The ground state two-neutron transfer only accounts for about 5% of this effect. In the no-coupling limit the cross section is 0.92 mb.

These features can be understood by considering the coupling form factors shown in Fig. 7. The upper part of this figure shows the potential barrier region relevant for the ^{28}Si + ^{64}Ni fusion reaction at $E_{c.m.} = 50$ MeV. The form factors in the lower part represent, in order of decreasing strength within the barrier, the projectile excitation, the bulk of the two-nucleon transfer, and the bulk of the one-nucleon transfer. This is the reason why the enhancement of the low energy fusion cross section due to these channels decreases in the same order. However, outside the barrier, in the classically allowed region, the one-nucleon transfer form factor is larger than that for two nucleons. Therefore the reflected flux in the one-nucleon channel will be larger. Of course, one also has to consider the excitation energies or Q values involved. For a fixed coupling strength, and within a reasonable range of Q values, the subbarrier fusion enhancement grows rapidly as the Q value becomes positive,[3] while the reflected flux peaks around the optimum Q value determined by the matching conditions at the turning point. As shown in Fig. 2, the two-nucleon transfer for ^{28}Si + ^{64}Ni has Q values which are less negative than the one-nucleon

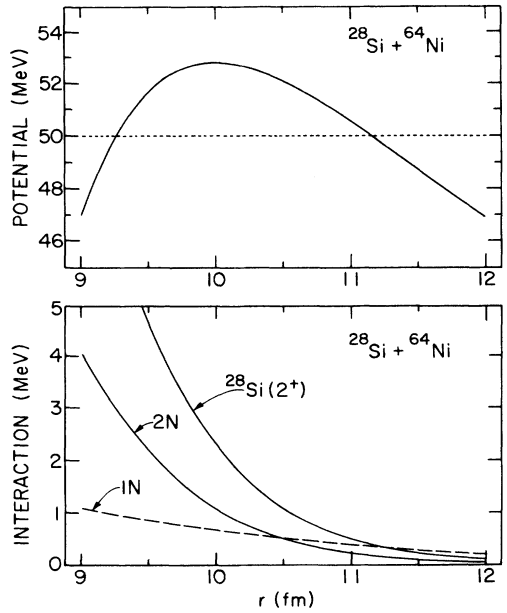

FIG. 7. Representation of the potential energy barrier and coupling interactions for ^{28}Si + ^{64}Ni. The interactions for the projectile excitation and the bulk of the two- and one-nucleon transfer reactions are indicated.

transfer.

The partial cross sections shown in Fig. 8 further illustrate the differences in the transfer reactions. The bulk of the single-nucleon transfer occurs for large partial waves due to its longer range form factor. It may also be noted that the one-nucleon transfer dominates the two-nucleon transfer for all partial waves, as one would expect from the ratio of the form factors at the s-wave turning point shown in Fig. 7. In contrast, the partial wave distribution of the fusion cross section shown in Fig. 8 does not reflect the range of a form factor, but is essentially controlled by the thickness of the potential barrier which is penetrated.

As a final point, we show in Fig. 9 how a small change in radius, as suggested by Hartree-Fock calculations, effect the fusion calculations for ^{30}Si + ^{64}Ni. The lower set

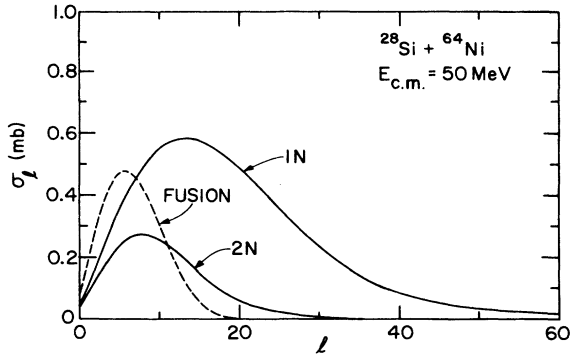

FIG. 8. Partial cross sections for fusion and one- and two-nucleon transfer reactions induced by ^{28}Si + ^{64}Ni at $E_{c.m.} = 50$ MeV.

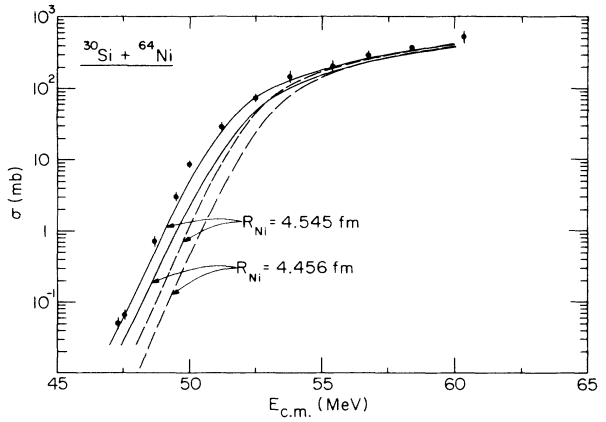

FIG. 9. Effect of the radius parameter on the ^{30}Si + ^{64}Ni fusion calculation. The solid and dashed curves show full-coupling and no-coupling results, respectively. The lower set of curves use a radius for ^{64}Ni which is scaled by $A^{1/3}$ from ^{58}Ni; in the upper ones the ^{64}Ni radius parameter is 2% larger.

of solid and dashed curves use a radius for ^{64}Ni which is scaled by $A^{1/3}$ from the radius of ^{58}Ni. For the upper set of curves, the ^{64}Ni radius parameter is increased by an additional 2%. This produces a significant increase in the fusion cross section, particularly at low energies, where the effect is comparable to the changes due to channel couplings.

It is interesting to note that this type of effect can be seen in the analysis of the ^{58}Ni + ^{58,64}Ni and ^{64}Ni + ^{64}Ni fusion reactions carried out in Ref. 21, where the potential radius was varied to fit the data. We have also checked that starting with a potential which reproduces the ^{58}Ni + ^{58}Ni fusion data above the barrier and using the $A^{1/3}$ scaling will lead to a significant underprediction of the higher energy ^{64}Ni + ^{64}Ni data. However, increasing the radius parameter an additional 2% gives a notably improved agreement. It may also be noted that a complementary effect was found in an analysis of the ^{40}Ca + ^{40,44,48}Ca fusion reactions.[22] In this case one does not expect the nuclear radii to increase as fast as $A^{1/3}$. Using such an increase in the potential, which gives agreement with the higher energy ^{40}Ca + ^{40}Ca data, leads to a significant overprediction of the corresponding ^{40}Ca + ^{48}Ca data.

IV. CONCLUSION

The subbbarrier enhancements of the fusion cross sections observed for the ^{28,30}Si + ^{58,62,64}Ni reactions have been reproduced by coupled-channels calculations. The calculations show that there is a significant and similar enhancement of the subbarrier cross sections for all of the cases due to the couplings to the low-lying inelastic excitations of the projectiles and targets. The strong projectile excitation gives the largest single contribution. The opposite signs of the deformations for ^{28}Si and ^{30}Si do not cause large effects.

The additional enhancements due to the transfer chan-

nels systematically improve the agreement between theory and experiment for the series of reactions and are essential for understanding the difference between the $^{28}Si + {}^{58,64}Ni$ cases. The main effect on the fusion from the transfer channels is predicted to come from the bulk of the two-neutron transfer. It is expected to be strongest for the case of $^{28}Si + {}^{64}Ni$, which has the least negative Q values. Although the one-nucleon transfers have relatively large cross sections, their influence on the subbarrier fusion rates are found to be small. An interesting result revealed by the systematics is that the fusion cross sections appear to reflect the details of the neutron radii predicted by Hartree-Fock calculations for the nickel isotopes.

The predicted transfer reaction cross sections at low excitation energies appear to have reasonable orders of magnitude. It would be an important check on the understanding of this series of fusion reactions to measure these transfer cross sections.

Recently,[23] transfer reactions have been measured for the $^{28}Si + {}^{58,62}Ni$ systems at an energy of about $E_{c.m.} = 75$ MeV. Although this energy is considerably higher than those we have considered, extrapolations of our calculations agree reasonably well with these measurements. In particular, the order of magnitude increase expected in the transfer cross section in going from the ^{58}Ni to the ^{62}Ni target is observed at the higher energy.

ACKNOWLEDGMENTS

It is a pleasure to thank H. Esbensen and K. E. Rehm for several helpful discussions. We are grateful to A. Brown at Michigan State University for supplying the Hartree-Fock results for the nickel isotopes. This work was supported by the U.S. Department of Energy under Contract No. W-31-109-ENG-38.

[1]A. M. Stefanini, G. Fortuna, A. Tivelli, W. Meczynski, S. Beghini, C. Signorini, S. Lunardi, and M. Morando, Phys. Rev. C **30**, 2088 (1984).
[2]S. Landowne and S. C. Pieper, Phys. Rev. C **29**, 1352 (1984).
[3]C. H. Dasso, S. Landowne, and A. Winther, Nucl. Phys. **A405**, 381 (1983); **A407**, 221 (1983).
[4]S. C. Pieper, M. J. Rhoades-Brown, and S. Landowne, Phys. Lett. **162B**, 43 (1985).
[5]T. Tamura, Rev. Mod. Phys. **37**, 679 (1965).
[6]P. R. Christensen, S. Pontoppidan, F. Videbaek, P. D. Bond, O. Hansen, C. E. Thorn, M. J. LeVine, and Jiang Cheng-Lie, Phys. Rev. C **28**, 159 (1983).
[7]R. A. Broglia and A. Winther, *Heavy Ion Reactions*, Lecture Notes (Benjamin, New York, 1981), Vol. I, p. 114.
[8]A. Brown, private communication.
[9]L. Ray, Phys. Rev. C **19**, 1855 (1979).
[10]C. H. Dasso and G. Pollarolo, Phys. Lett. **155B**, 223 (1985).
[11]R. A. Broglia, C. H. Dasso, and S. Landowne, Phys. Rev. C **32**, 1426 (1985).
[12]R. A. Broglia, R. Liotta, B. S. Nilsson, and A. Winther, Phys. Rep. **29c**, 291 (1977).
[13]W. P. Alford, R. N. Boyd, E. Sugarbaker, D. L. Hanson, and E. R. Flynn, Phys. Rev. C **21**, 1203 (1980).
[14]F. Videbaek, Ole Hansen, B. S. Nilsson, E. R. Flynn, and J. C. Peng, Nucl. Phys. **A433**, 441 (1985).
[15]K. E. Rehm, in Proceedings of the Symposium on the Many Facets of Heavy-Ion Fusion Reactions, Argonne, 1986, Argonne National Laboratory Report ANL-PHY-86/1.
[16]R. A. Broglia, C. H. Dasso, S. Landowne, and A. Winther, Phys. Rev. C **27**, 2433 (1983).
[17]Nuclear Data Tables **28**, 559 (1979).
[18]P. M. Endt and C. Van der Leun, Nucl. Phys. **A310**, 1 (1978).
[19]Nuclear Data Tables **47**, 135 (1986).
[20]Nuclear Data Tables **47**, 1 (1986).
[21]M. Beckerman, M. Salomaa, A. Sperduto, J. D. Molitoris, and A. DiRienzo, Phys. Rev. C **25**, 837 (1982).
[22]S. Landowne, C. H. Dasso, R. A. Broglia, and G. Pollarolo, Phys. Rev. C **31**, 1047 (1985).
[23]Y. Sugiyama, Y. Tomita, H. Ikezoe, K. Ideno, N. Shikazono, N. Kato, H. Fujita, T. Sugimitsu, and S. Kubono, Phys. Lett. **176B**, 302 (1986).